

# Silicon Carbide Metasurfaces for Controlling the Spontaneous Emission of Embedded Color Centers

Mohammed Ashahar Ahamad and Faraz Ahmed Inam

Department of Physics, Aligarh Muslim University, Aligarh, Uttar Pradesh 202002, India  
faraz.inam.phy@amu.ac.in

Stefania Castelletto

School of Engineering, RMIT University, Melbourne, Victoria 3001, Australia  
Stefania.castelletto@rmit.edu.au

**Abstract:** Nanopillars fabricated in diamond or silicon-carbide (SiC) have been used to enhance the light harvesting or absorption or to increase the collection efficiency of embedded single photon emission in the visible or near infrared for their detection using confocal microscopy. While electric and magnetic dipolar resonances in SiC have been studied in the far-infrared, they have not been studied in the near infrared. Here we show for the first time that electromagnetic Mie-scattering moments within SiC metasurfaces can control the spontaneous emission process of point defects in the near infrared. Using SiC nanopillars based metasurfaces, we theoretically demonstrate a control over the spontaneous emission rate of embedded color-centers by using the coherent superposition of the electric dipolar and magnetic quadrupolar electromagnetic Mie-scattering moments of the structure. More than an order of magnitude emission/decay rate enhancement is obtained with the maximum enhancement close to 30. We also demonstrate that the relative phase of the Mie-scattering moments helps in controlling the emission directionality. SiC metasurfaces in the spectral range of color centres, from the visible to the near infrared, can be used to control the confinement and directionality of their spontaneous emission, increasing the opportunities to study light-matter interaction and to advance quantum photonic and quantum sensing device integration.

**Keywords:** Mie-scattering moments, silicon carbide nanopillars metasurface, emission enhancements, radiation directionality, color centres

© 2022 The Author(s)

## 1. Introduction

Color-centers in silicon-carbide (SiC) are example of emitters that possess single photon emission [1], optical spin read out and control, and have been amongst the most studied for optical coherence spin control and spin-photon interface [2, 3] due to their very long coherence time [4, 5] and photo-stability. SiC is quite distinguished from the other material platforms as it possesses color centre with optical-spin properties combined with advanced material fabrication methods, metal-oxide-semiconductor functionalities [6] and nonlinear second and third order optical properties. Due to its wide electronic bandgap which leads to broad optical transparency, photostable color centres emission [7] which extend to the near infrared, CMOS compatibility [8] and availability of quantum-grade wafer-scale SiC on insulator, it has emerged as one of the most promising material for integrated quantum photonic applications [9, 10].

In particular, SiC can host a wide range of point defects/color centers including silicon vacancy  $V_{Si}$  (V1, V2, V3), divacancies  $V_{Si}V_C$  and carbon antisite vacancy pair  $C_{Si}V_C$  [11]. The  $V_{Si}$  in SiC is a promising single photon source (SPS) for spin-photon interface in the near infrared region around 917nm [12, 13]. At present the main challenge in applying SiC for quantum networks is to significantly enhance the rate of single photon generation and collection from embedded color-centers. Photonics is mainly used to enhance the properties of these systems.

So far in SiC bulk material, nanopillars have been fabricated to enhance the light harvesting or collection efficiency of embedded single photon emission for their detection using confocal microscopy [12, 14]; while meta-lenses [15] are used to modify the phase front of the emitted light, achieving high focusing and large emission directionality of the color-centers emitting below these meta-lenses. Currently metasurfaces used to excite/enhance

the magnetic and electric resonances in SiC have been investigated only in the far infrared [16] and in the context of surface phonon polaritons studies [17]. Recently it has been shown that metamaterial/metasurface light matter interaction can be used to control, enhance and tune the quantum properties of bulk materials [18, 19]. In particular all dielectric metasurfaces due to their zero absorption losses have emerged as the preferred platform compared to plasmonics in photo-luminescence enhancement [20]. When a dielectric structure is placed under electromagnetic excitation, various charge and current distributions are excited in it. These distributions results in multi-polar Mie-scattering resonances being excited in structures with dimensions of the order of the excitation wavelength [21]. A coherent superposition of these resonances leads to many interesting phenomena like, bound states in continuum (BIC) [22], tuning of the radiation directionality in the lateral or transverse directions [23] and tuning of the local optical density of states (LDOS) to achieve emission rate enhancement for emitters embedded in the metasurfaces [24].

Here for the first time we study the electric dipolar and magnetic quadrupolar resonances in the near infrared in SiC for controlling the spontaneous emission rate of the embedded color centers in the dielectric nanopillars forming Mie resonators.

In this study, using the coherent superposition of Mie-scattering resonances in SiC pillars based metasurface, we theoretically demonstrate that it is possible to control the spectral spontaneous emission process of the embedded color-centers. We first optimise the scattering efficiency of the SiC metasurface when excited by a plane wave and then by a dipole emitter. In the case the light source is a dipole, namely the  $V_{Si}$  embedded in the SiC metamaterial, we study the effects of the metasurface based on array of nanopillars Mie resonances on the LDOS and emission directionality. In particular, we study the effect of the periodicity of the nanopillars array to increase the emission rate and maintain high directionality compared to the case of a single pillar.

## 2. Theoretical background

Scattering is the phenomenon of re-emission of radiation by a particle after undergoing interaction with radiation [25]. When a plane electromagnetic wave is incident on a particle, charge distribution and displacement currents  $\mathbf{J}(\mathbf{r}) = -i\omega\epsilon_0(\epsilon_r - 1)\mathbf{E}(\mathbf{r})$  (here  $\mathbf{E}(\mathbf{r})$  is the field at the position vector  $\mathbf{r}$ ,  $\omega = 2\pi\nu$  is the angular frequency,  $\epsilon_r$  and  $\epsilon_0$  are the permittivity of the particle and surrounding medium) are excited within it. When the particle's dimensions are of the order of the excitation wavelength, the excited charge and current distributions leads to the development of multipolar Mie-scattering modes [26, 27]. The amplitude and phase of excitation of the electric and magnetic resonances or multi-polar Mie-scattering moments inside the scatterer are totally governed by its size, shape and surrounding electromagnetic environment [28]. These multi-polar Mie resonances in the visible spectral range have been demonstrated experimentally in the last decade using a silicon spherical nanoparticles and nanodiamonds [29, 30].

The total scattering efficiency (SE)  $C_{sca}^{total}$  is calculated by normalizing the total far field scattered power to the energy flux of the incident wave on the scatterer [31]. The total SE  $C_{sca}^t$  is the sum of partial SE from different multipoles:  $C_{sca}^p$ ,  $C_{sca}^m$ ,  $C_{sca}^Q$  and  $C_{sca}^M$  represents contributions from electric dipole, magnetic dipole, electric quadrupole and magnetic quadrupole respectively [32].

$$C_{sca}^{total} = C_{sca}^p + C_{sca}^m + C_{sca}^Q + C_{sca}^M \quad (1)$$

$$C_{sca}^{total} = \frac{k^4}{6\pi\epsilon_0^2|E_{inc}|^2} \left[ \sum \left( |p_\alpha|^2 + \left| \frac{m_\alpha}{c} \right|^2 \right) + \frac{1}{120} \sum \left( |kQ_{\alpha\beta}^e|^2 + \left| \frac{kQ_{\alpha\beta}^m}{c} \right|^2 \right) \right] \quad (2)$$

where,  $p_\alpha$  and  $m_\alpha$  are the electric and magnetic dipole moments with  $Q_{\alpha\beta}^e$  and  $Q_{\alpha\beta}^m$  being the corresponding quadrupole moments.  $|E_{inc}|$  is the amplitude of the incident electric field,  $k$  is the wave-vector and  $c$  is the speed of light. They are mathematically expressed as [32]:

$$ED : p_\alpha = -\frac{1}{i\omega} \left\{ \int d^3\mathbf{r} \mathbf{J}_\alpha^\omega j_0(kr) + \frac{k^2}{2} \int d^3\mathbf{r} [3(\mathbf{r} \cdot \mathbf{J}_\omega) r_\alpha - r^2 J_\alpha^\omega] \frac{j_2(kr)}{(kr)^2} \right\} \quad (3)$$

$$MD : m_\alpha = \frac{3}{2} \int d^3\mathbf{r} (\mathbf{r} \times \mathbf{J}_\omega)_\alpha \frac{j_1(kr)}{kr} \quad (4)$$

$$EQ : Q_{\alpha\beta}^e = -\frac{3}{i\omega} \left\{ \int d^3\mathbf{r} [3(r_\beta J_\alpha^\omega + r_\alpha J_\beta^\omega) - 2(\mathbf{r} \cdot \mathbf{J}_\omega) \delta_{\alpha\beta}] \frac{j_1(kr)}{(kr)} \right. \\ \left. + 2k^2 \int d^3\mathbf{r} [5r_\alpha r_\beta (\mathbf{r} \cdot \mathbf{J}_\omega) - (r_\alpha J_\beta + r_\beta J_\alpha) r^2 - r^2 (\mathbf{r} \cdot \mathbf{J}_\omega) \delta_{\alpha\beta}] \frac{j_3(kr)}{(kr)^3} \right\} \quad (5)$$

$$MQ : Q_{\alpha\beta}^m = 15 \int d^3\mathbf{r} \left\{ r_\alpha (\mathbf{r} \times \mathbf{J}_\omega)_\beta + r_\beta (\mathbf{r} \times \mathbf{J}_\omega)_\alpha \right\} \frac{j_2(kr)}{(kr)^2} \quad (6)$$

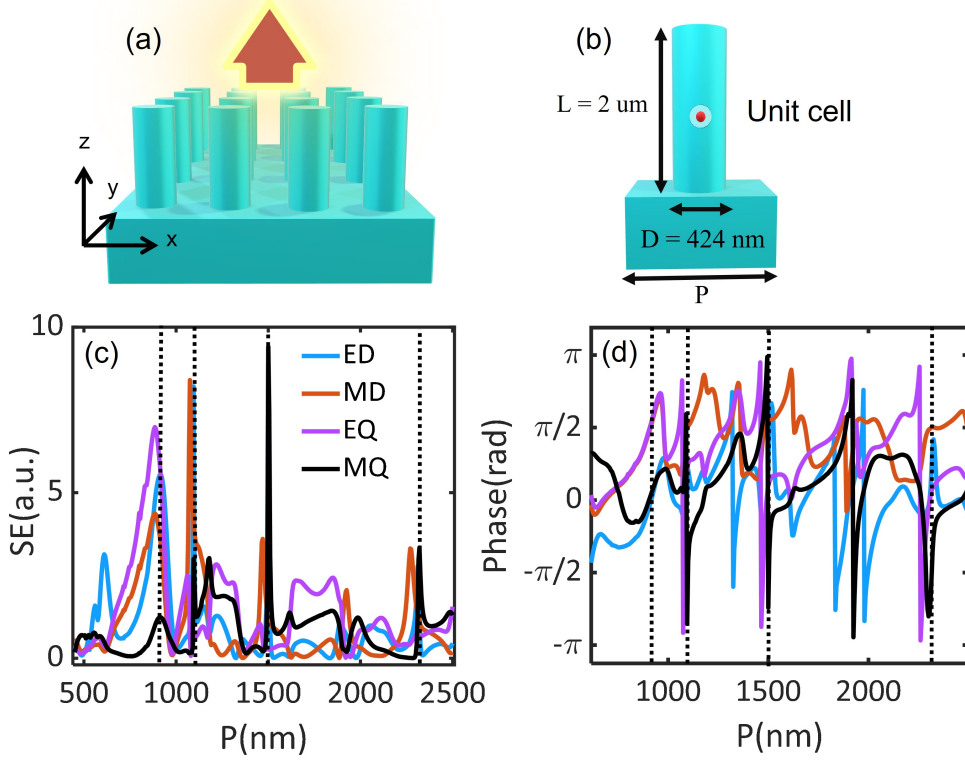


Fig. 1. (a) Schematic of the metasurface with a 2D periodic lattice of SiC pillars under plane-wave excitation at 917 nm with wave-vector along the +z-direction. (b) Schematic of the unit cell. Each pillar has a length  $L = 2 \mu\text{m}$  and diameter  $D = 424 \text{ nm}$  with a dipole emitter located at the center of each pillar. (c) The SE of the individual multipolar Mie-scattering moments as a function of the lattice periodicity,  $P$ , under plane-wave excitation at 917 nm.  $P$  is varied from 450 nm to 2500 nm. (d) The corresponding phase of the individual multipolar Mie-scattering moments as a function of the lattice periodicity,  $P$ . The dotted black lines corresponds to overlapping ED and MQ resonances with  $P = 915 \text{ nm}$ ,  $1095 \text{ nm}$ ,  $1500 \text{ nm}$  and  $2315 \text{ nm}$ .

The Mie-resonances control the electromagnetic field amplitudes within the scatterer and therefore contribute in tuning the local electromagnetic density of states (LDOS). The LDOS due to the local electromagnetic environment around a point dipole emitter is defined as [33]

$$\rho(\omega, r) = \sum_{k, \sigma} |\hat{d} \cdot \mathbf{E}_{k, \sigma}(r)|^2 \delta(\omega - \omega_{k, \sigma}). \quad (7)$$

Here,  $\hat{d}$  is the unit vector specifying the direction of the transition dipole moment with  $\omega$  being the transition frequency. The summation is over all wavevectors ( $k$ ) and polarizations ( $\sigma$ ).  $\mathbf{E}$  is the total electric field at the source position resulting from the superposition of the fields directly radiated by the dipole emitter embedded inside the scatterer with the fields reflected and scattered back from the surroundings. The LDOS govern the complete radiation process of a dipole emitter. Hence the Mie-scattering modes play a vital role in tuning the spontaneous emission process of the emitter by controlling the scattered electric field at the source point.

The balancing of the electric and magnetic Mie-scattering moments leads to the directionality of the scattered radiation pattern [32]. The radiation pattern is controlled by the relative phase of the balanced electric and magnetic multi-polar moments [34]. When the electric and magnetic dipolar moments are balanced and in phase,  $|ED| = |MD|$ ,  $\arg(ED) = \arg(MD)$ , this leads to a completely forward radiation directionality, known as the Kerker condition [32]. When these dipolar moments are out-of-phase,  $|ED| = |MD|$ ,  $\arg(ED) = \arg(MD) + \pi$ , it results in a completely backward directionality, known as the anti-Kerker condition [34]. When the superposition of dipolar

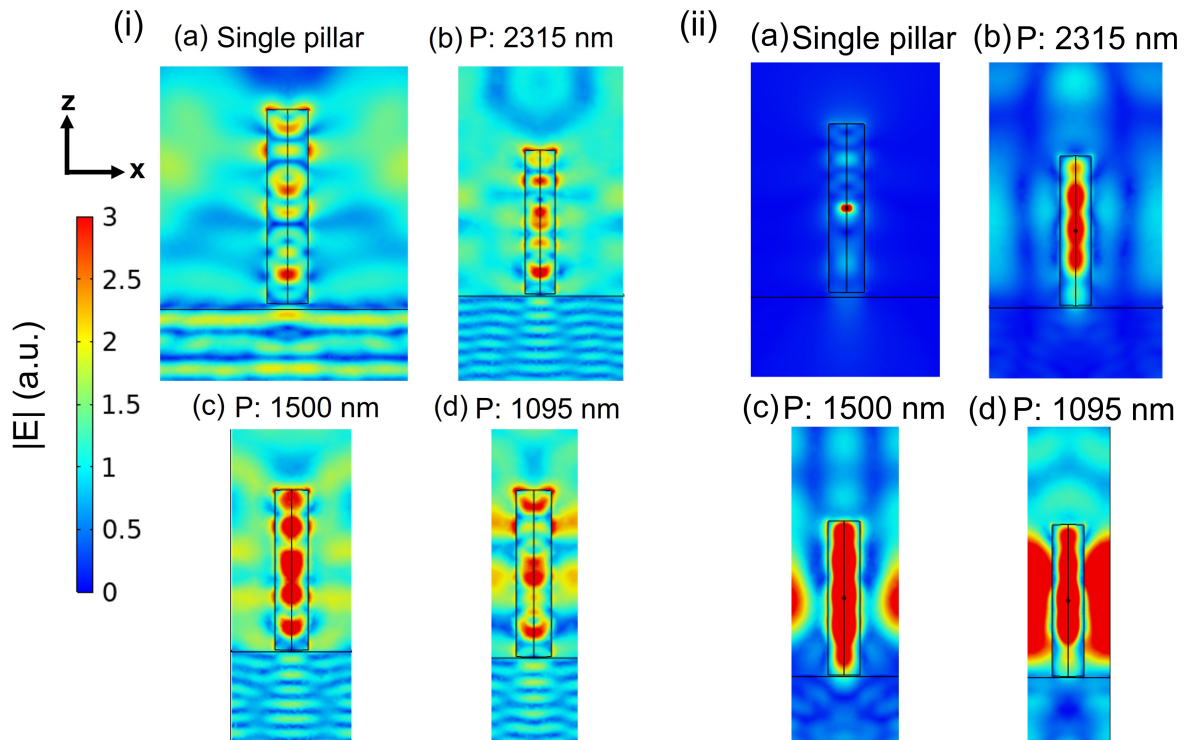


Fig. 2. The 2D electric field norm within (a) a single SiC pillar and the SiC pillar metasurface with  $P =$  (b) 2315 nm, (c) 1500 nm and (d) 1095 nm under (i) plane wave excitation with wave-vector along the  $+z$ -direction and electric field polarized along the  $+x$ -direction and (ii) dipole excitation with dipole emitter placed at the center of the SiC pillar with orientation along the  $x$ -direction.

as well as the quadrupolar moments are balanced and are in phase,  $|ED + MD| = |EQ + MQ|$  with  $\arg(ED + MD) = \arg(EQ + MQ)$ , the radiation pattern is highly directional along the forward direction, known as the generalised Kerker condition [34]. However, when these superpositions are out-of-phase, this leads to a complete transverse scattering [34]. The phase of the Mie-scattering moments therefore controls the far-field scattering radiation pattern of the scatterer. Under a point dipole emitter excitation of the structure, the far-field scattering pattern of the structures also influences the radiation pattern of the dipole emitter placed in the vicinity of the scatterer [35].

In the following we investigate these effects in SiC nanopillars array under plane wave-excitation and under a single dipole excitation simulating the  $V_{\text{Si}}$ .

### 3. Results and discussion

#### 3.1. Scattering efficiency and decay-rate enhancement

We have computationally optimised the SiC metasurface, shown in Fig. 1(a) with unit cell in Fig. 1(b), to achieve the generalised Kerker's condition in SiC for the specific color centre of interest. The metasurface consists of a periodic 2D lattice of SiC pillars, each of length,  $L = 2\mu\text{m}$ . The electrodynamics calculations are performed using the commercial Comsol Multiphysics RF module. The details of the calculations are presented in the Methods sections. The metasurface is excited by a plane wave with wavelength,  $\lambda_{exc}$ , travelling along the  $+z$ -direction (arrow symbol in Fig. 1(a)) with the electric field polarized along the  $+x$ -direction. Under the influence of the plane electromagnetic wave, Mie scattering moments are excited within the SiC pillars. We first optimised the diameter,  $D$ , of the SiC pillars for the maxima in the SE at  $\lambda_{exc} = 917$  nm corresponding to the zero phonon line (ZPL) of the silicon vacancy,  $V_{\text{Si}}$  in SiC [36,37]. The optimised  $D$  value was found to be around 424 nm. We then study the coherent superposition of the Mie-scattering modes of the individual SiC pillars by varying the lattice periodicity,  $P$ . For  $P \gg \lambda_{exc}$ , the structure is expected to behave as a single isolated pillar. With decreasing  $P$ , the interactions between the Mie-scattering modes of the individual pillars will increase. When these modes will be in phase, their coherent superposition will lead to a maxima for the total SE of the 2D SiC pillar lattice. Fig. 1(c) and (d) show the amplitude and the phase of the individual Mie-scattering moments of the SiC pillar metasurface as a function of  $P$ . Sharp resonance peaks are observed in the amplitude of the individual Mie-scattering moments

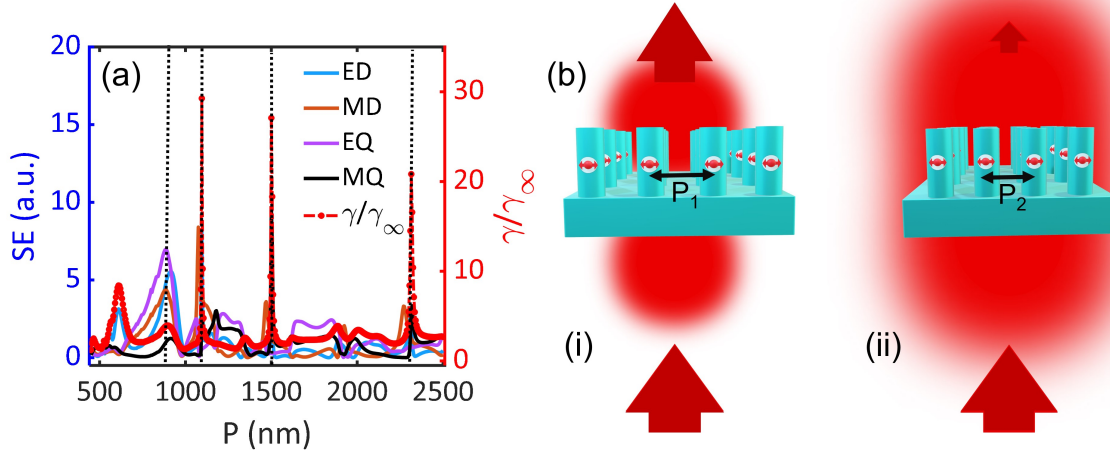


Fig. 3. The SE of the individual excited multipolar Mie-scattering moments and the emitter's ( $V_{Si}$  color-center) relative decay rate in the SiC pillar metasurface as a function of the lattice periodicity,  $P$ . The dipole emitter is placed at the center of the SiC pillars with dipole orientation along the horizontal plane. The  $\gamma_\infty$  is the emitter's decay rate in the bulk SiC. (b) The schematic representation of the tuning of the embedded color-center's emission with the lattice periodicity,  $P$  set to (i) off-resonant  $P_1$  and (ii) resonant  $P_2$  values.

(Fig. 1(c)). At these sharp resonances, a sharp jump in the phase of the corresponding Mie-scattering moment is observed (Fig. 1(d)). We will now focus on the local maxima arising due to the ED and the MQ moments (under dipole excitation of the structure only these two resonances were excited and were observed to have an influence on the dipole emitter's decay rates). These local maxima are observed for  $P = 915$  nm,  $1095$  nm,  $1500$  nm and  $2315$  nm (black dotted lines in Fig. 1(c) and (d)). At  $P = 915$  nm, the ED resonance peak is much greater than the MQ resonance with the phase of these two resonances being equal. For  $P = 1095$  nm,  $1500$  nm and  $2315$  nm, the ED and MQ moments are nearly balanced and a sharp jump is also observed in their phase. We will now examine the balanced superposition of these two moments at  $P = 1095$  nm,  $1500$  nm and  $2315$  nm.

Figure 2(i) shows the normalised electric field distribution within a (a) single SiC pillar and the SiC pillar metasurface with  $P =$  (b)  $2315$  nm, (c)  $1500$  nm and (d)  $1095$  nm under plane wave excitation with wave-vector along the  $+z$ -direction and electric field polarized along the  $+x$ -direction. Strong confinement of the electric field within the SiC cylinder is observed at these  $P$  values corresponding to the balanced superposition of the ED and MQ resonances, with the maximum field confinement observed for  $P = 1500$  nm (the SE was also observed to be maximum at this  $P$  value). The field confinement will in-turn lead to LDOS enhancement within the SiC pillar (Eq 7). For a dipole emitter placed at the field maxima points, the LDOS enhancement will lead to its decay rate enhancement. Figure Fig. 2(ii) shows the normalised electric field distribution within (a) a single SiC pillar and the SiC pillar metasurface with  $P =$  (b)  $2315$  nm, (c)  $1500$  nm and (d)  $1095$  nm under dipole excitation with dipole emitter placed at the center of the SiC pillars with orientation along the  $x$ -direction. Large field confinement/enhancement which will lead to large LDOS enhancement can be observed here.

We now study the influence of the above LDOS enhancement on the spontaneous emission rates of a dipole emitter, the  $V_{Si}$  color-center embedded at the center of each SiC pillar. Figure 3(a) shows the emitter's ( $V_{Si}$  color-center) relative decay rate together with the SE of the individual Mie-scattering moments in the SiC pillar metasurface as a function of the lattice periodicity,  $P$ . The decay rates of the  $V_{Si}$  emitter in the SiC pillar metasurface,  $\gamma$  are scaled relative to its decay rates in a bulk SiC crystal,  $\gamma_\infty$ . The influence of the LDOS enhancement arising from the electric field confinement (Fig. 2) in tuning the emitter's decay rate can be clearly observed here. Also, it can be observed that the relative decay rates ( $\frac{\gamma}{\gamma_\infty}$ ) (dash-dotted red curve) only tunes with the local maxima which are dominated by ED and MQ resonances. These resonances corresponds to  $P = 1095$  nm,  $1500$  nm and  $2315$  nm, respectively. A schematic representation of the embedded dipole emitter's radiation tuning with the SiC pillar lattice periodicity,  $P$  at an off-resonant (i) and resonant (ii) value is presented in Fig. 3.

In Fig. 4, we study the SE spectral response due to all the excited Mie-scattering moments and the effect on the relative decay rates of a horizontally oriented (along  $x$ -direction) dipole source for the above resonant

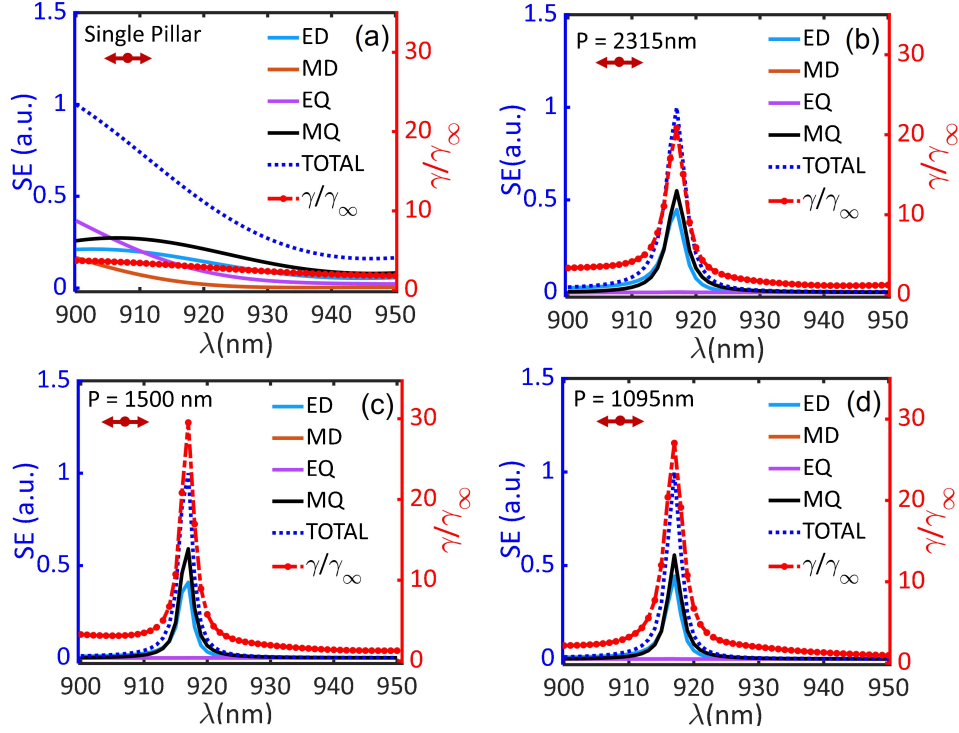


Fig. 4. The spectral response of the SE with the individual excited multipolar Mie-scattering moments under horizontal dipole excitation and the emitter's ( $V_{Si}$  color-center with dipole orientation along the horizontal plane) relative decay rate in a (a) single SiC pillar; SiC pillar metasurface with  $P =$  (b) 2315nm, (c) 1500 nm and (d) 1095 nm, respectively.

periodicity values ( $P = 1095$  nm, 1500 nm and 2315 nm) of the metasurface. Here, the Mie-scattering moments of the metasurface are excited by the dipole source itself. For an isolated SiC pillar (Fig. 4(a)), all the studied Mie-scattering moments are observed to be weakly excited with no clear resonances. The relative decay rate (dash-dotted red curve) is observed to be around 2.7 at 917 nm. However, for all resonant  $P$  values ( $P = 1095$  nm, 1500 nm and 2315 nm), significant contributions are observed only from the ED and MQ moments. Their superposition is controlling the behaviour of the SE and the relative decay rate. The maximum relative decay rate enhancement is close to 30 at 917 nm for  $P = 1500$  nm and 1095 nm. For  $P = 2315$  nm the enhancement is about 20. Therefore, it can be concluded that the coherent superposition of the ED and MQ Mie-scattering moments of the individual pillars are enhancing the decay rates of an embedded dipole emitter by more than an order of magnitude.

We now study the role of the phase of the excited Mie-scattering moments (ED and MQ) of the SiC pillar metasurface on the far field radiation pattern of an embedded dipole emitter.

### 3.2. Phase analysis and Radiation pattern

Figure 5 shows a narrow range of values for both the relative amplitudes and phase of the ED and MQ moments at the resonant  $P$  values. At the  $V_{Si}$  color-center's peak emission wavelength of 917 nm, the MQ moment appears to be slightly larger than the ED moment. For  $P = 1500$  nm, the  $\frac{ED}{MQ} = 0.7$  and for  $P = 1095$  nm and 2315 nm, the  $\frac{ED}{MQ} = 0.81$ . The corresponding phase difference between ED and MQ moments is  $\pi$  at 917 nm for all resonant  $P$  values.

In Fig. 6(i) we show the in-phase and out-of-phase superposition of the balanced ED and MQ moments. The influence of this superposition on both the in-plane (X-Z plane, blue curve) and out-of-plane (Y-Z plane, red curve) far-field scattering patterns is shown here. The in-phase ( $ED + MQ$ ) superposition results in longitudinal (along top and bottom directions) scattering and the out-of-phase ( $ED - MQ$ ) superposition results in transverse scattering along the out-of-plane direction (red curve).

We now study the influence of the ED and MQ moments superpositions on the embedded dipole emitter radiation pattern for a single nanopillar and SiC metasurface of array of interacting nanopillars. The emitter's dipole orientation is along the X-direction. Fig. 6(ii) shows the far-field emission patterns of the embedded  $V_{Si}$  color-

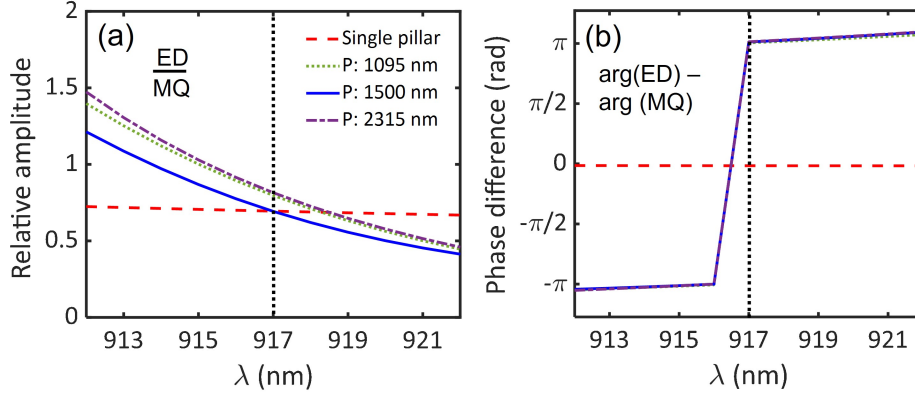


Fig. 5. The spectral response of the (a) relative amplitudes and (b) phase difference of the electric dipolar (ED) and magnetic quadrupolar (MQ) Mie-scattering moments excited under horizontal dipole excitation.

center at 917 nm for different resonant  $P$  values. In a single pillar, the majority of the emission is observed to be directed towards the bottom surface and lies mainly along the longitudinal direction (bottom and top). However, in the SiC metasurface at the resonant  $P$  values corresponding to ED and MQ moments, the out-of-phase superposition of the ED and MQ moments (the phase difference between these moments was observed to be close to  $\pi$  at 917 nm in Fig. 5) directs the embedded emitter's radiation pattern along the transverse direction, especially in the out-of-plane (Y-Z plane, red curve).

#### 4. Conclusion

We studied for the first time the coherent superposition of the electric and magnetic dipolar and quadrupolar Mie-scattering moments of SiC metamaterial nanopillars array in the near infrared emission (917 nm). We first determined the design of the metasurface periodicity to induce sharp resonances in the amplitude and phase of the Mie-scattering moments. Strong electric field confinement was observed within the SiC pillar when the periodicity of the lattice matched with the resonance of the ED and MQ modes. The field confinement leads to large LDOS and subsequently decay rate enhancement for a color-center dipole embedded at the center of the SiC pillar. Under a point dipole emitter excitation within SiC, it was determined that only the ED and MQ moments are contributing to the electromagnetic scattering in the SiC nanopillars metasurface. Both these moments were observed to be nicely coupled and were showing collective resonance at the optimized wavelength (917 nm). The coherent superposition of these two moments controls the complete spontaneous emission process of the embedded color center. At the collective resonance point of these two moments ( $\lambda = 917$  nm), we determined more than an order of magnitude decay rate enhancement with the maximum enhancement reaching 30. Such an enhancement has never been reported in dielectric neither in metal-dielectric individual nanopillars [38], thus paving the way for the use SiC metasurfaces to enhance and control light extraction from quantum emitters, to study light-matter interaction effects in integrated quantum photonics and for applications in quantum sensing. We also observed that by designing specific resonant structures, the coherent superposition of the ED and MQ moments can be used to better control the radiation/emission pattern and hence the emission directionality of the embedded dipole emitter compared to a single nanopillar. Specifically the embedded emitter's radiation pattern can be more confined along the transverse direction, especially in the out-of-plane (Y-Z plane, red curve), thus facilitating the planar emission propagation. Such result is relevant for applications of SiC metasurfaces for planar integrated photonics. Our study can prompt further studies on SiC quantum states of light based on multi-emitters-resonators coupling enabled by metamaterials such as superradiance [39].

#### 5. Materials and Methods

All the electrodynamic calculations have been performed using the commercial COMSOL Multiphysics Radio Frequency (RF) module. The periodic boundary conditions are applied to all the horizontal planes defining the 2D lattice of the SiC substrate to build an array of dielectric pillars metasurface. The scattering boundary conditions are applied at the top and bottom boundaries of the computational domain. The optical constant for the SiC has been extracted from the experimentally reported values by Singh et al. [40]. During the entire calculation the minimum meshing size was 1 nm with the maximum being  $\lambda/7$ .

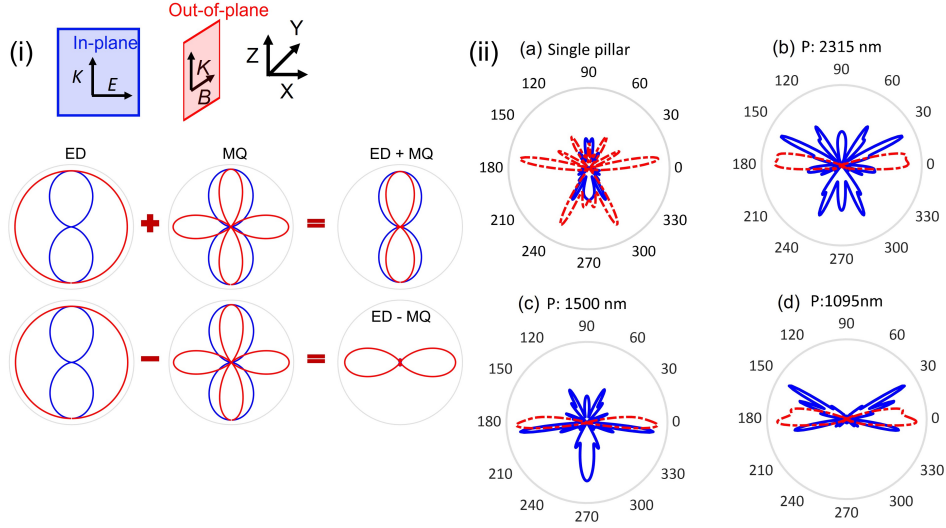


Fig. 6. (i) In-plane (X-Z plane, blue curves) and out-of-plane (Y-Z plane, red curves) far-field scattering pattern corresponding to the in-phase (ED+MD) and out-of-phase (ED-MQ) superposition of the electric dipolar (ED) and magnetic quadrupolar (MQ) Mie-scattering moments. (ii) Farfield radiation patterns in-plane (X-Z plane, blue curves) and out-of-plane (Y-Z plane, red curves) of a dipole emitter (orientation along the X-direction, same as that of electric field in (i)) placed at the center of (a) single pillar; SiC pillar metasturface with  $P =$  (b) 2315nm, (c) 1500 nm and (d) 1095 nm, respectively.

### 5.1. Scattering efficiency calculation

The scattering cross section is defined as the amount of power scattered by the scatterer to the amount of power per unit area carried by the incident wave. The SE is obtained just by dividing the scattering cross-section by the geometrical cross-section. Mathematically it is expressed as  $SE = \sigma_s/G$  [41]. Here  $\sigma_s$  is the scattering cross section and  $G$  is geometrical cross section.

The SE is calculated semi-analytically using electric field values at each mesh point in the computational grid under plane-wave excitation using Comsol Multi-physics module. Using these field values and permittivity profile at each mesh points, current density is calculated as:  $J_\omega(r) = i\omega\epsilon_0(\epsilon_r - 1)E_\omega(r)$ . Here  $\epsilon_0$  and  $\epsilon_r$  are permittivity of free space and SiC medium, respectively. The computationally obtained values of  $E(r)$ ,  $J_\omega(r)$  and  $\epsilon(r)$  are used to calculate individual multipolar Mie-scattering moments,  $p_\alpha$ ,  $m_\alpha$ ,  $Q_{\alpha\beta}^e$  and  $Q_{\alpha\beta}^m$  described in Eq. 2. The integration referred in Eq. 2 is carried on the domain of the SiC pillar.

### 5.2. Relative decay rate calculations

In these calculations, the SiV center is treated as a classical radiating point dipole source. In the computational domain, it is modelled as a point current source driven at the emission frequency,  $\nu = \frac{c}{\lambda}$  [42]. Scattering/perfectly matched layer (PML) boundary conditions are applied on the exterior boundaries of the computational domain. The total power radiated by the dipole is integrated over a closed surface enclosing the current source. The relative decay-rate is calculated as  $\Gamma_{rel} = \gamma/\gamma_\infty = P/P_\infty$  [42], where  $P_\infty$  is the power corresponding to the point dipole's emission in the bulk SiC. The permittivity of SiC is taken from [43].

**Acknowledgement** The authors would like to acknowledge the financial support from the Department of Science and Technology (DST), India (CRG/2021/001167). The authors thank Dr Nadeem Ahmed for his help regarding the plotting of the figures and the formatting of the manuscript. MA and FAI also thank Dr Ahmed Mekawy for his help regarding multipole decomposition of the Mie-scattering moments.

### References

1. A. Lohrmann, B. C. Johnson, J. C. McCallum, and S. Castelletto, "A review on single photon sources in silicon carbide," Reports on Prog. Phys. **80**, 034502 (2017).
2. D. D. Awschalom, R. Hanson, J. Wrachtrup, and B. B. Zhou, "Quantum technologies with optically interfaced solid-state spins," Nat. Photonics **12**, 516–527 (2018).



3. N. T. Son, C. P. Anderson, A. Bourassa, K. C. Miao, C. Babin, M. Widmann, M. Niethammer, J. Ul-Hassan, N. Morioka, I. G. Ivanov *et al.*, “Developing silicon carbide for quantum spintronics,” *Appl. Phys. Lett.* **116**, 190501 (2020).
4. C. P. Anderson, E. O. Glen, C. Zeledon, A. Bourassa, Y. Jin, Y. Zhu, C. Vorwerk, A. L. Crook, H. Abe, J. Ul-Hassan, T. Ohshima, N. T. Son, G. Galli, and D. D. Awschalom, “Five-second coherence of a single spin with single-shot readout in silicon carbide,” *Sci. Adv.* **8**, eabm5912 (2022).
5. D. Simin, H. Kraus, A. Sperlich, T. Ohshima, G. V. Astakhov, and V. Dyakonov, “Locking of electron spin coherence above 20 ms in natural silicon carbide,” *Phys. Rev. B Condens. Matter.* **95**, 161201 (2017).
6. G. Liu, B. R. Tuttle, and S. Dhar, “Silicon carbide: A unique platform for metal-oxide-semiconductor physics,” *Appl. Phys. Rev.* **2**, 021307 (2015).
7. S. Castelletto, “Silicon carbide single-photon sources: challenges and prospects,” *Mater. for Quantum Technol.* **1**, 023001 (2021).
8. Y. Zhu, W. Wei, A. Yi, T. Jin, C. Shen, X. Wang, L. Zhou, C. Wang, W. Ou, S. Song *et al.*, “Hybrid integration of deterministic quantum dots-based single-photon sources with cmos-compatible silicon carbide photonics,” arXiv preprint arXiv:2203.12202 (2022).
9. D. M. Lukin, M. A. Guidry, and J. Vučković, “Integrated quantum photonics with silicon carbide: challenges and prospects,” *PRX Quantum* **1**, 020102 (2020).
10. S. Castelletto, A. Peruzzo, C. Bonato, B. C. Johnson, M. Radulaski, H. Ou, F. Kaiser, and J. Wrachtrup, “Silicon carbide photonics bridging quantum technology,” *ACS Photonics* **9**, 1434–1457 (2022).
11. S. Castelletto and A. Boretti, “Silicon carbide color centers for quantum applications,” *J. Physics: Photonics* **2**, 022001 (2020).
12. M. Radulaski, M. Widmann, M. Niethammer, J. L. Zhang, S.-Y. Lee, T. Rendler, K. G. Lagoudakis, N. T. Son, E. Janzén, T. Ohshima, J. Wrachtrup, and J. Vučković, “Scalable Quantum Photonics with Single Color Centers in Silicon Carbide,” *Nano Lett.* **17**, 1782–1786 (2017).
13. N. Morioka, C. Babin, R. Nagy, I. Gediz, E. Hesselmeier, D. Liu, M. Joliffe, M. Niethammer, D. Dasari, V. Vorobyov *et al.*, “Spin-controlled generation of indistinguishable and distinguishable photons from silicon vacancy centres in silicon carbide,” *Nat. communications* **11**, 1–8 (2020).
14. S. Castelletto, A. S. Al Atem, F. A. Inam, H. J. von Bardeleben, S. Hameau, A. F. Almutairi, G. Guillot, S.-i. Sato, A. Boretti, and J. M. Bluet, “Deterministic placement of ultra-bright near-infrared color centers in arrays of silicon carbide micropillars,” *Beilstein J. Nanotechnol.* **10**, 2383–2395 (2019).
15. O. Schaeper, Z. Yang, M. Kianinia, J. E. Fröch, A. Komar, Z. Mu, W. Gao, D. N. Neshev, and I. Aharonovich, “Monolithic Silicon Carbide Metalenses,” *ACS Photonics* **9**, 1409–1414 (2022).
16. J. A. Schuller, R. Zia, T. Taubner, and M. L. Brongersma, “Dielectric metamaterials based on electric and magnetic resonances of silicon carbide particles,” *Phys. Rev. Lett.* **99**, 107401 (2007).
17. J. D. Caldwell, O. J. Glembocki, Y. Francescato, N. Sharac, V. Giannini, F. J. Bezares, J. P. Long, J. C. Owrutsky, I. Vurgaftman, J. G. Tischler *et al.*, “Low-loss, extreme subdiffraction photon confinement via silicon carbide localized surface phonon polariton resonators,” *Nano Lett.* **13**, 3690–3697 (2013).
18. C.-W. Qiu, T. Zhang, G. Hu, and Y. Kivshar, “Quo vadis, metasurfaces?” *Nano Lett.* **21**, 5461–5474 (2021).
19. A. S. Solntsev, G. S. Agarwal, and Y. S. Kivshar, “Metasurfaces for quantum photonics,” *Nat. Photonics* **15**, 327–336 (2021).
20. Y.-T. Lin, A. Hassanfiroozi, W.-R. Jiang, M.-Y. Liao, W.-J. Lee, and P. C. Wu, “Photoluminescence enhancement with all-dielectric coherent metasurfaces,” *Nanophotonics* **11**, 2701–2709 (2022).
21. R. Alaei, C. Rockstuhl, and I. Fernandez-Corbaton, “An electromagnetic multipole expansion beyond the long-wavelength approximation,” *Opt. Commun.* **407**, 17–21 (2018).
22. Z. Liu, Y. Xu, Y. Lin, J. Xiang, T. Feng, Q. Cao, J. Li, S. Lan, and J. Liu, “High-Q Quasibound States in the Continuum for Nonlinear Metasurfaces,” *Phys. Rev. Lett.* **123** (2019).
23. H. K. Shamkhi, K. V. Baryshnikova, A. Sayanskiy, P. Kapitanova, P. D. Terekhov, P. Belov, A. Karabchevsky, A. B. Evlyukhin, Y. Kivshar, and A. S. Shalin, “Transverse scattering and generalized kerker effects in all-dielectric mie-resonant metaoptics,” *Phys. Rev. Lett.* **122**, 193905 (2019).
24. M. Khokhar, F. A. Inam, and R. V. Nair, “Kerker Condition for Enhancing Emission Rate and Directivity of Single Emitter Coupled to Dielectric Metasurfaces,” *Adv. Opt. Mater.* **10**, 2200978 (2022).
25. H. C. Hulst and H. C. van de Hulst, *Light scattering by small particles* (Courier Corporation, 1981).
26. G. Mie, “Contributions to the optics of turbid media, particularly of colloidal metal solutions,” *Contributions to optics turbid media* **25**, 377–445 (1976).
27. F. J. Bezares, J. P. Long, O. J. Glembocki, J. Guo, R. W. Rendell, R. Kasica, L. Shirey, J. C. Owrutsky, and J. D. Caldwell, “Mie resonance-enhanced light absorption in periodic silicon nanopillar arrays,” *Opt. Express* **21**, 27587–27601 (2013).
28. C. F. Bohren and D. R. Huffman, *Absorption and scattering of light by small particles* (John Wiley & Sons, 2008).
29. A. B. Evlyukhin, S. M. Novikov, U. Zywietz, R. L. Eriksen, C. Reinhardt, S. I. Bozhevolnyi, and B. N. Chichkov, “Demonstration of magnetic dipole resonances of dielectric nanospheres in the visible region,” *Nano letters* **12**, 3749–3755 (2012).
30. D. A. Shilkin, M. R. Shcherbakov, E. V. Lyubin, K. G. Katamadze, O. S. Kudryavtsev, V. S. Sedov, I. I. Vlasov, and A. A. Fedyanin, “Optical magnetism and fundamental modes of nanodiamonds,” *ACS Photonics* **4**, 1153–1158 (2017).

31. T. Hinamoto and M. Fujii, "Menp: an open-source matlab implementation of multipole expansion for nanophotonics," *Osa Continuum* **4**, 1640–1648 (2021).
32. R. Alaei, R. Filter, D. Lehr, F. Lederer, and C. Rockstuhl, "A generalized Kerker condition for highly directive nanoantennas," *Opt. Lett.* **40**, 2645 (2015).
33. F. Inam, T. Gaebel, C. Bradac, L. Stewart, M. Withford, J. Dawes, J. Rabeau, and M. Steel, "Modification of spontaneous emission from nanodiamond colour centres on a structured surface," *New J. Phys.* **13**, 073012 (2011).
34. H. K. Shamkhi, K. V. Baryshnikova, A. Sayanskiy, P. Kapitanova, P. D. Terekhov, P. Belov, A. Karabchevsky, A. B. Evlyukhin, Y. Kivshar, and A. S. Shalin, "Transverse scattering and generalized kerker effects in all-dielectric Mie-resonant metaoptics," *Phys. review letters* **122**, 193905 (2019).
35. F. Qin, Z. Zhang, K. Zheng, Y. Xu, S. Fu, Y. Wang, and Y. Qin, "Transverse kerker effect for dipole sources," *Phys. Rev. Lett.* **128**, 193901 (2022).
36. F. Fuchs, B. Stender, M. Trupke, D. Simin, J. Pflaum, V. Dyakonov, and G. V. Astakhov, "Engineering near-infrared single-photon emitters with optically active spins in ultrapure silicon carbide," *Nat. Commun.* **6**, 7578 (2015).
37. M. Widmann, S. Y. Lee, T. Rendler, N. T. Son, H. Fedder, S. Paik, L. P. Yang, N. Zhao, S. Yang, I. Booker, A. Denisenko, M. Jamali, S. Ali Momenzadeh, I. Gerhardt, T. Ohshima, A. Gali, E. Janzén, and J. Wrachtrup, "Coherent control of single spins in silicon carbide at room temperature," *Nat. Mater.* **14**, 164–168 (2015).
38. F. A. Inam and S. Castelletto, "Metal-dielectric nanopillar antenna-resonators for efficient collected photon rate from silicon carbide color centers," *Nanomaterials* **13** (2023).
39. O. Mello, Y. Li, S. A. Camayd-Muñoz, C. DeVault, M. Lobet, H. Tang, M. Lonçar, and E. Mazur, "Extended many-body superradiance in diamond epsilon near-zero metamaterials," *Appl. Phys. Lett.* **120**, 061105 (2022).
40. S. Singh, J. Potopowicz, L. Van Uitert, and S. Wemple, "Nonlinear optical properties of hexagonal silicon carbide," *Appl. Phys. Lett.* **19**, 53–56 (1971).
41. F. Frezza, F. Mangini, and N. Tedeschi, "Tutorial: Introduction to electromagnetic scattering," *J. Opt. Soc. Am. A* **31**, 1–11 (2017).
42. Y. Xu, J. S. Vučković, R. K. Lee, O. J. Painter, A. Scherer, and A. Yariv, "Finite-difference time-domain calculation of spontaneous emission lifetime in a microcavity," *J. Opt. Soc. Am. B* **16**, 465 (1999).
43. P. T. B. Shaffer, "Refractive Index, Dispersion, and Birefringence of Silicon Carbide Polytypes," *Appl. Opt. Vol. 10, Issue 5*, pp. 1034–1036 **10**, 1034–1036 (1971).